Transactions, SMiRT-26
Berlin/Potsdam, Germany, July 10-15, 2022
Division I

THE FRACTURE ENERGY OF FIBRE REINFORCED CONCRETE UNDER HIGH STRAIN RATES

Oliver Mosig[1], Vahan Zohrabyan[2], Manfred Curbach[3] and Thomas Braml[4]

[1] Dr.-Ing., Inst. of Concrete Structures, Dresden, oliver.mosig@tu-dresden.de

[2] M. Eng., Inst. of Concrete Structures, Neubiberg, vahan.zohrabyan@unibw.de

[3] Prof. Dr.-Ing. Dr.-Ing. E.h., Inst. of Concrete Structures, Dresden, manfred.curbach@tu-dresden.de

[4] Prof. Dr.-Ing., Inst. of Concrete Structures, Neubiberg, thomas.braml@unibw.de

ABSTRACT

Fibre-reinforced concrete can offer decisive advantages for the dimensioning of structures against dynamic loadings such as explosions or impact. On the one hand, increasing ductility increases the deformability and also the energy absorption capacity. On the other hand, fibres can prevent flying debris. In this study, the material properties of fibre-reinforced concrete such as modulus of elasticity, tensile strength and fracture energy were determined based on spalling tests in the split Hopkinson bar. Concretes of the strength classes C20/25, C40/50 and C80/95 with steel fibre contents of 0 to 2.0 vol.-% and also with carbon and PP fibres were investigated. The results show an increase in the dynamic tensile strength and the dynamic modulus of elasticity with increasing fibre content. The addition of fibres also leads to an enormous increase in fracture energy, which is higher for steel fibres compared to carbon and PP fibres. Parts of this article were already published in Mosig et al. (2021).

INTRODUCTION

Fibre-reinforced concrete is characterized by a high ductility compared to normal concrete. The fibres form a kind of discontinuous, three-dimensionally oriented, isotropic reinforcement in the concrete. They bridge cracks at very small crack widths, transfer loads and develop post-cracking strength in concrete (Strack (2007), Holschemacher et al. (2002)). As a result, large displacements are required for failure (separation) of a fibre-reinforced concrete specimen under direct tensile loading compared to unreinforced normal concrete. For the dimensioning of buildings or structures against highly dynamic loads, such as explosions or vehicle impact, these properties can bring decisive advantages (Hering (2020), Zohrabyan et al. (2020)). On the one hand, the increasing ductility increases the deformation capacity and thus also the energy absorption of the component. On the other hand, the resulting flying debris can be prevented and persons inside the building can be protected (Zircher et al. (2016), Fuchs et al. (2007)).

In order to understand the behaviour of fibre-reinforced concretes under dynamic loading, knowledge of the governing dynamic mechanical properties such as tensile strength, modulus of elasticity and fracture energy is required, Gebbeken et al. (2008). Within the scope of the experimental investigations, these values were determined by dynamic spalling tests in a split Hopkinson bar (SHB). Concretes of the strength classes C20/25, C40/50 and C80/95 with steel fibre contents of 0 to 2.0 vol.-% alternatively with 1.0 vol.-% of carbon and PP fibres were investigated.

MATERIAL AND SPECIMENS

For the spalling tests, cylindrical specimens with a diameter of 50 mm and a comparatively large length of about 470 mm were used to introduce the longest possible loading waves into the specimen without superposition, so that sufficient energy was available to separate the fibre-reinforced specimens. The concrete mixes used (see Table 1) have a maximum grain size of 8 mm. The production of the concrete and fibre-reinforced concrete specimens is based on the current standards for concrete construction DIN EN 12620, DIN 1045 2, DIN EN 206-1, DIN EN 14889-1 and the DAfStb guideline for steel fibre-reinforced concrete. After stripping, the specimens were stored in water at 20 °C for 28 days.

Cylinder specimens with the following characteristics were prepared and tested for the spalling tests:

- Steel fibre types: DRAMIX with C20/25 & C30/37 and KrampeHarex with C80/95 (Table 2, Figure 1), fibre contents: 0/0.5/1.0 and 2.0 vol.-%,
- PP and carbon fibres with C40/50 (Table 2, Figure 1), fibre content: 1.0 vol.-%.

Table 1. Concrete composition [kg/m³]

Concrete	Cement	Water	Sand 0/4	Gravel 4/8	w/c-ratio
C20/25	240 (CEM I 42,5 R)	180	1,561	413	0.75
C40/50	350 (CEM I 52,5 R)	175	1,519	395	0.5
C80/95	550 (CEM I 52,5 R)	165	1,034	347	0.3
Concrete	Cement	Water	Sand 0/2	Gravel 2/8	w/c-ratio
C30/37	280 (CEM I 52,5 R), 70 (fly ash)	160	923	965	0.45

Table 2. Fibre types

Fibre type	Length [mm]	Diameter [mm]	Tensile strength [N/mm²]	Modulus of elastic [N/mm²]
Dramix (steel fibre)	35	0.55	1,850	200,000
KrampeHarex (steel fibre)	35	0.55	2,000	210,000
MasterFiber 236 (PP fibre)	29	0.75	469	4,000
DURA (carbon fibre)	12	0.007	4,000	240,000

Figure 1. Fibre types: steel fibres a) Dramix and b) KrampeHarex, c) Carbon fibre, d) PP fibre

Some of the specimens had a 4 mm deep notch at a distance of 175 mm from the end of the specimen (Figure 2). This notch can provoke failure in the test and reduce the probability of the occurrence of a multiple crack pattern. In addition, unnotched spallation specimens were also investigated, which are more suitable for determining the tensile strength, Weerheijm and Vegt (2010). For each configuration 4 unnotched and 4 notched specimens were investigated.

Figure 2. Specimens for the spalling tests

STATIC TESTS

For the evaluation of the SHB tests, knowledge of the corresponding static material properties is essential. Therefore, static reference tests (compressive strength DIN EN 12390-3:2009, split tensile strength DIN EN 12390-6:2010, modulus of elasticity DIN EN 12390-13:2014 etc.) were carried out (see Table 3).

Table 3. Static material parameters (mean values)

Concrete	Fibre content [vol.-%]	Fibre type	Compressive strength [N/mm²]	Tensile strength [N/mm²]	Modulus of elasticity [N/mm²]
C20/25	0.0	-	31.4	1.83	28,844
	0.5	DRAMIX	34.7	2.63	30,878
	1.0	DRAMIX	35.8	2.50	20,752
	2.0	DRAMIX	33.6	3.14	22,586
C30/37	0.0	-	38,9	2.90	31,304
	0.5	DRAMIX	41.1	2.95	32,503
	1.0	DRAMIX	42.0	4.05	31,157
	2.0	DRAMIX	41.7	4.20	30,029
C40/50	1.0	Carbon fibre	66.2	5.20	35,881
	1.0	PP fibre	61.6	5.41	31,211
C80/95	0.0	-	83.4	5.36	40,432
	0.5	KrampeHarex	90.4	6.14	40,317
	1.0	KrampeHarex	63.0	7.25	45,337
	2.0	KrampeHarex	87.9	7.13	45,323

DYNAMIC TESTS

Test and measuring setup

In the spalling test, an impactor hits the input bar with the velocity v_{Imp} and thus generates a pressure wave (ε_{Ind}), which propagates along the input bar at the speed of sound c (Figure 3). At the interface between the input bar and the specimen, the difference in impedance causes a partial reflection (ε_{Ref}) and a partial transmission of the wave into the concrete specimen (ε_{Tra}). This pressure wave passes through the specimen and reflects at the free end as a tensile wave. Outside the superposition region of the transmitted compression wave and the reflected tensile wave, the resulting tensile wave leads to spalling failure. The specimen cracks and the fragments move away from each other due to their remaining kinetic energy.

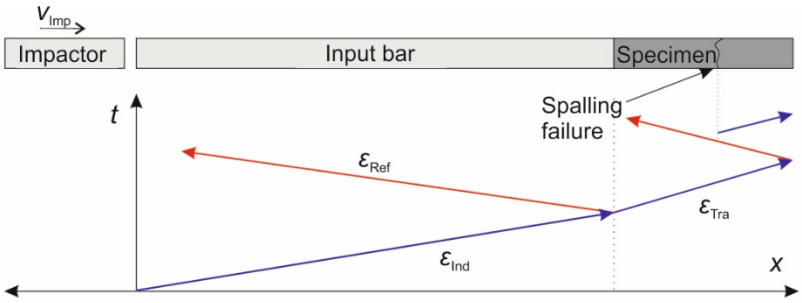

Figure 3. Principle of the spalling experiment

For the measurement two high-speed cameras (HSK), an extensometer and strain gauges (DMS 1 and DMS 2) were used (Figure 4). One high-speed camera (HSK 1: 100,000 fps, 128 × 320 pixels) was placed directly at the notch so that the temporal evolution of the crack opening due to the spalling failure could be recorded. The second high-speed camera (HSK 2: 20,000 fps, 320 × 1024 pixels) filmed the complete specimen during the test. The impactor velocities ranged from 6 to 10.5 m/s, depending on the type of concrete (concretes with a higher fibre content were tested with higher impactor velocities). The projectile was a cylindrical aluminium impactor (d_{Imp} = 50 mm) with a length of 250 mm.

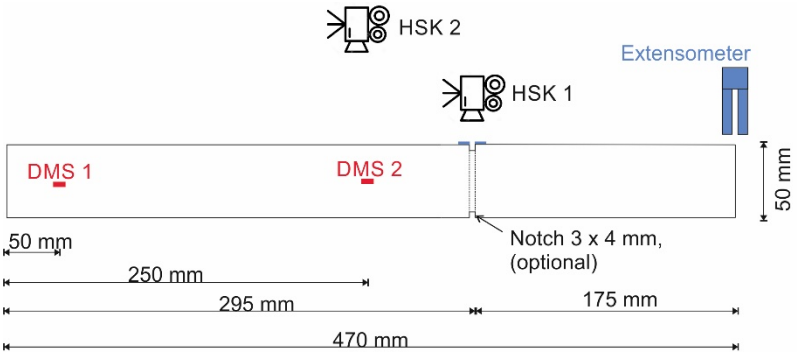

Figure 4. Measuring arrangement in the spallation test; incoming pressure wave from the left

RESULTS

Modulus of elasticity

The dynamic modulus of elasticity is calculated with the recordings of the strain gages. A 6th order Blackman low-pass filter with a frequency of 40 kHz was used for data processing (Kühn et al. (2016)).

Due to the known distance between the two strain gages ΔL_{DMS} of 200 mm, the velocity c through the specimen can be determined with the time offset Δt and the dynamic modulus of elasticity E can be calculated with c and the density ρ:

$$c = \frac{\Delta L_{DMS}}{\Delta t} \tag{1}$$

$$E = c^2 \cdot \rho \tag{2}$$

The dynamic moduli of elasticity are given as mean values in Table 4. With increasing fibre content, a slight increase in the dynamic modulus of elasticity can be observed. This can be partly explained by the higher density of the steel fibre-reinforced specimens and has also been observed in static investigations, Gul et al. (2014).

Table 4. Test results (mean values), values in brackets: specimens with failure in the notch

Concrete	Fibre content [vol.-%]	E [kN/mm²]	f_t [N/mm²]	$\dot{\varepsilon}$ [1/s]	$G_{F,A}$ [N/m]
C20/25	0.0	31.1	9.03 (12.41)	19.4	253
	0.5	33.1	8.77 (10.47)	15.9	1,600
	1.0	34.2	9.24 (12.85)	19.4	2,110
	2.0	33.1	9.02 (12.20)	18.7	2,506
C30/37	0.0	31.1	6.67 (11.18)	15.1	234
	0.5	31.1	7.60 (13.67)	21.1	1,586
	1.0	32.1	9.12 (11.03)	17.3	2,512
	2.0	32.5	8.13 (12.57)	22.4	2,685
C40/50 C	1.0	40.7	9.68 (17.07)	18.0	809
C40/50 PP	1.0	42.9	10.20	20.9	1,177
C80/95	0.0	43.5	13.18 (22.12)	20.9	309
	0.5	44.6	14.05 (26.08)	25.7	2,228
	1.0	45.7	15.62 (23.41)	28.3	3,576
	2.0	48.7	16.86 (24.34)	24.7	4,009

Tensile strength

The tensile strength of the specimen f_t is determined from the change in the particle velocity at the free end of the specimen, the pullback velocity v_{pb} (Figure 5), Meyers (1994) and Zukas (1990). For this purpose, an extensometer was used, which records the displacement of the free end and by its derivation, the particle velocity can be determined:

$$f_t = \frac{1}{2} \cdot c \cdot \rho \cdot v_{pb} \cdot \frac{A}{A_n} \tag{3}$$

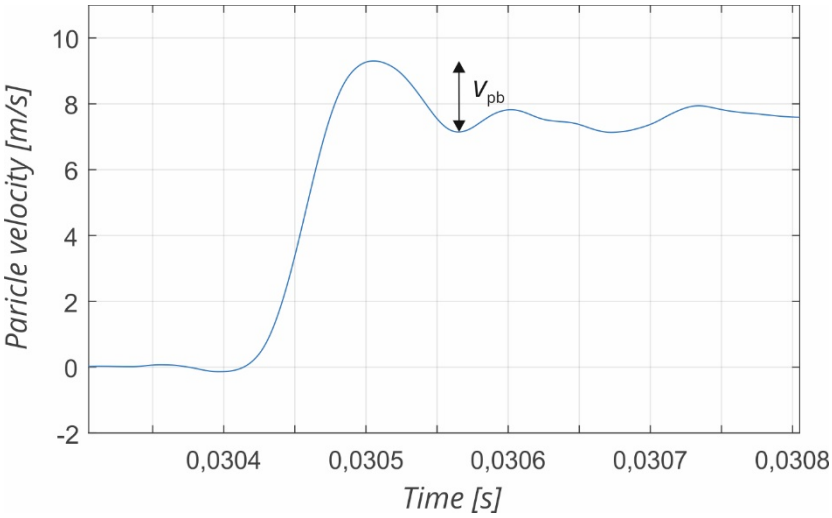

Figure 5. Particle velocity at the free end from the extensometer data

The factor A/A_n describes the ratio of the cross-sectional area of specimen A to the cross-sectional area in notch A_n (if the failure occurred in the notch). The associated strain rate $\dot{\varepsilon}$ is obtained from the measured particle velocity v at the free end of the specimen:

$$\dot{\varepsilon} = \frac{d\varepsilon}{dt} = \frac{dv}{2 \cdot c\, dt} \tag{4}$$

Table 4 shows the average values of the calculated tensile strengths. The values in brackets correspond to the tensile strengths of the notched specimens with failure inside the notch area. In the test series of the C40/50 PP, no tensile strength could be determined on the notched specimens. The higher tensile strength of notched specimens compared to unnotched specimens has already been observed in Schuler (2004), among others. According to Weerheijm and Vegt (2010), the determination of the dynamic tensile strength on unnotched specimens is preferable. As under static loading, an increase in dynamic tensile strength can be observed with increasing fibre content (Shankar et al. (2018). Due to the increased loading rate (strain rates in the range of 15 to 25 1/s), a significant increase in strength is also evident compared to static loading (strain rate effect) (Bischoff and Perry (1986), Mosig and Curbach (2019 and 2020)).

Fracture

The resulting fracture pattern is of decisive importance for the determination of the fracture energy G_F. Based on the spalling tests, 6 different fracture patterns (denoted in the following by FM: failure mode) could be observed (Table 5). The fracture energy can only be determined if the fragment is completely separated from the rest of the specimen at the free end (FM 1, 3 and 5). If the fragment at the free end is still connected to the remaining fragment (crack but no separation, or crack and subsequent separation in the fragment), no fracture energy can be determined (FM 2, 4 and 6).

In a total of 74 out of 105 tests carried out, a fracture pattern suitable for the determination of the fracture energy could be determined.

Table 5: Failure modes (FM) of the spalling specimens (incoming wave from the right)

FM	Fracture	G_F
1		✓
2		✗
3		✓
4		✗
5		✓
6		✗

Fracture energy

The fracture energy is calculated from the momentum transfer during the fracture process. A very detailed description of this methodology can be found in Schuler (2004) and Millon et al. (2009). This momentum transfer results from the velocity change of the fractured piece Δv_i, the fractured piece mass m_i as well as the average crack opening velocity $\emptyset\delta'_{crack}$:

$$G_F = \Delta v_i \cdot m_i \cdot \emptyset\delta'_{crack} \tag{5}$$

After carrying out the test, the fracture masses and lengths are known. As described above, the fracture energy was determined only in failure modes 1, 3 and 5 and usually at the fracture plane closest to the free end (between fracture piece (FP) 1 and FP 2). For the determination of the velocity change of a FP, the fragment velocity before and after the fracture is necessary:

$$\Delta v_i = v_{i,before} - v_{i,after} \tag{6}$$

The images from the high-speed cameras are used to determine the two velocities using GOM Aramis software. The crack opening velocity δ'_{crack} was determined in the same way and results from the velocity difference of two neighboring fragments:

$$\delta'_{crack} = v_i - v_{i+1} \tag{7}$$

Figure 6 and Figure 7 show the velocities as well as the crack opening velocity between FP1 and FP2 for an unreinforced and a steel fibre-reinforced (2.0 vol.-%) specimen, respectively.

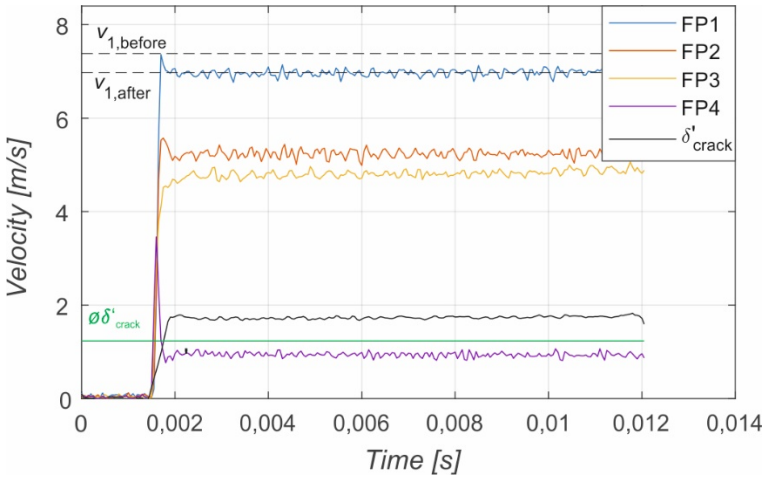

Figure 6. Velocities of fragments FP1–4 and crack opening velocity (unreinforced specimen)

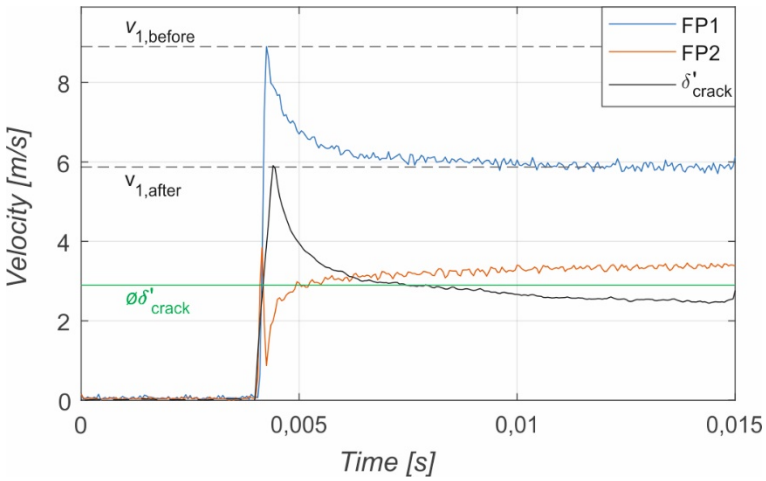

Figure 7. Velocities of fragments and crack opening velocity (2.0 vol.-% steel fibre reinforced specimen)

The velocity before fracture $v_{1,before}$ corresponds to the maximum in the velocity progression of fracture 1. The velocity after fracture $v_{1,after}$ occurs when the failure process is complete. This can be seen from the fact that the crack opening velocity between FP1 and FP2 is constant as soon as the two fragments are completely separated from each other. The average crack opening velocity $Ø\delta'_{crack}$ is then calculated as the average value of the crack opening velocity δ'_{crack} from the region of the beginning of the failure (δ'_{crack} = 0) to the complete separation (δ'_{crack} = constant) of the fragments. In the crack opening velocities (and also in the individual fragment velocities), clear differences in the progression can be seen in the comparison of fibre-reinforced to unreinforced specimens (Figure 6 and Figure 7). In the case of unreinforced specimens, the fragment velocities and thus also the crack opening velocity are almost constant after crack formation. In contrast, the velocity curves of fibre-reinforced concrete specimens show larger and longer-lasting changes as a result of fibre pullout or fibre fracture. The greater the velocity drop of the fragment, the higher the fracture energy.

Knowing the change in velocity of fracture piece 1 and the crack opening velocity, the fracture energy can then be determined according to equation 5. For the specific fracture energy $G_{F,A}$, the previously calculated fracture energy is related to the cross-sectional area in the fracture zone A_B (notched or unnotched

cross-sectional area). The specific fracture energies determined are shown in Figure 8 in their individual values; Table 4 again contains the mean values.

$$G_{F,A} = \frac{G_F}{A_B} \tag{8}$$

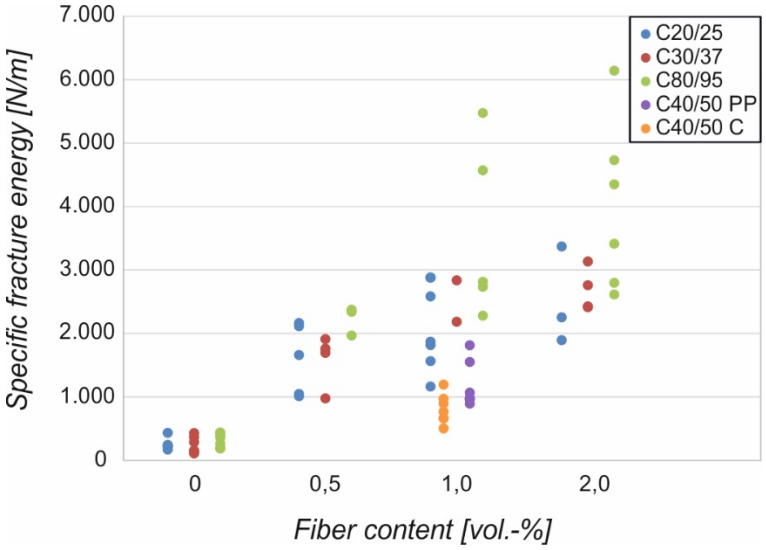

Figure 8. Determined specific fracture energies as a function of fibre content

The specific fracture energies of the unreinforced concrete specimens are in the range of 200 to 300 N/m and are comparable with values from Weerheijm and Van Doormal (2007). The addition of steel fibres leads to a significant increase of the fracture energy, which further increases with increasing fibre content. At a fibre content of 1.0 vol.-%, a tenfold increase in fracture energy is thus possible compared to the unreinforced specimens. The investigated alternative carbon and PP fibres (1.0 vol.-%) also lead to an increase in the fracture energy compared to concrete specimens without short fibre addition, which is, however, lower at 800 N/m and 1200 N/m, respectively, than for the steel fibre-reinforced specimens (~ 2500 N/m at 1.0 vol.-%).

CONCLUSION

In the study presented here, the dynamic parameters modulus of elasticity, tensile strength and fracture energy were determined based on spallation tests of fibre-reinforced concrete specimens in the split Hopkinson bar. It was found that an increase in the modulus of elasticity and tensile strength of the fibre-reinforced concrete results from an increase in the volume content of fibre. Furthermore, the addition of steel fibres increased the fracture energy enormously (tenfold at 1.0 vol.-% compared with unreinforced specimens), with an increased fibre content causing a higher increase. The alternatively investigated carbon and PP fibres also led to an increase in the fracture energy of concrete specimens, which, however, was lower compared to steel fibre-reinforced specimens. The objective of reducing or eliminating flying debris in impact-loaded components mentioned at the beginning can be achieved by adding fibres. This suitability is now to be further verified through large-scale component tests.

ACKNOWLEDGEMENT

The project was funded by the German Federal Ministry for Economic Affairs and Energy on the basis of a resolution of the German Bundestag under the funding code 1501581.

REFERENCES

Bischoff, P. H., Perry, S. H. (1986). *Compressive Strain Rate Effects of Concrete*. MRS Proceedings (64), p. 151 – 165.

Fuchs, M., Keuser, M., Schuler, H., Thoma, K. (2007). *Faserbeton unter hochdynamischer Einwirkung*. Beton- und Stahlbetonbau 102 11, p. 759–769.

Gebbeken, N., Greulich, S., Pietzsch, A., Hartmann, T. (2008). *Modellbildung zur Simulation von Stahlfaserbeton unter hochdynamischer Belastung*. Beton- und Stahlbetonbau 103 6, 2008, p. 398-412.

Gul, M., Bashir, A., Naqash, J. A. (2014). *Study of Modulus of Elasticity of Steel Fiber Reinforced Concrete*. Intern. Journal of Engineering and Advanced Techn. 3, H. 4, p.304–309.

Hering, M. (2020). *Untersuchung von mineralisch gebundenen Verstärkungsschichten für Stahlbetonplatten gegen Impaktbeanspruchungen*. Dissertation, TU Dresden.

Holschemacher, K., Dehn, F. (2002). *Faserbeton – ein innovativer Baustoff auf dem Weg in die Zukunft*. In: König, Holschemacher, Dehn: Faserbeton. Innovationen im Bauwesen.

Hummeltenberg, A., Kühn, T., Just, M., Quast, M., Curbach, M., Häussler-Combe, U. (2013). *Verhalten von Beton bei hohen Belastungsgeschwindigkeiten – Experimentelle Untersuchungen zur zweiaxialen Festigkeit und Formulierung einer stoffgesetzlichen Beschreibung*. Forschungsbericht, IMB der TU Dresden.

Kühn, T., Steinke, C., Sile, Z., Zreid, I., Kaliske, M., Curbach, M. (2016). *Dynamische Eigenschaften von Beton im Experiment und in der Simulation*. Beton- und Stahlbetonbau 111, Heft 1, p. 41–50.

Meyers, M. A. (1994). *Dynamic Behaviour of Materials*. John Wiley & Sons.

Millon, O., Riedel, W., Thoma, K., Fehling, E., Nöldgen, M. (2009). F*iber-reinforced ultra-high performance concrete under tensile loads*. Proc. of DYMAT 2009, Brüssel, p. 671–677.

Mosig, O., Curbach, M. (2019). *Einfluss der Wassersättigung auf die statische und dynamische Druckfestigkeit von Beton*. Beton- und Stahlbetonbau 114, H 3, p. 168-175.

Mosig, O.; Curbach, M. (2020). *The crack propagation velocity as a reason for the strain rate effect of concrete — An analytical model*. Civil Engineering Design 2, H 4, p. 123-130.

Mosig, O., Zohrabyan, V., Curbach, M., Braml, T., Keuser, M.; Gebbeken, N. (2021) *Spallationsversuche von Faserbetonprobekörpern im Split-Hopkinson-Bar.* Beton- und Stahlbetonbau 116, H. 6, p. 468–477.

Quast, M. (2019). *Zweiaxiale Betondruckfestigkeit unter hohen Belastungsgeschwindigkeiten.* Dissertation, TU Dresden.

Schuler, H. (2004) *Experimentelle und numerische Untersuchungen zur Schädigung von stoßbeanspruchtem Beton*. Dissertation, Universität der Bundeswehr München.

Shankar, H., Khare, P., Khan, M. A. (2018). *A Review on Tensile Behavior of Steel Fiber Reinforced Concrete*. Intern. Res. J. of Eng. and Techn. (IRJET) 05, H. 05, p. 2196–2198.

Strack, M. (2007). M*odellbildung zum rissbreitenabhängigen Tragverhalten von Stahlfaserbeton unter Biegebeanspruchung*. Dissertation, Ruhr-Universität Bochum.

Weerheijm, J., Van Doormal, J. C. A. M. (2007). Tensile failure of concrete at high loading rates: New test data on strength and fracture energy from instrumented spalling tests. Int. J. of Impact Engineering 34, p. 609–626.

Weerheijm, J., Vegt, I. (2010). *The dynamic fracture energy of concrete. Review of test methods and data comparison*. Proc. of FraMCoS-7, Jeju Island (Korea), 2010, p. 419–427.

Zircher, T., Michal, M., Keuser, M., Burbach, A. (2016). *Use of steel fiber concrete for protective components*. Proc. of 24th MABS, Paper 80, Halifax, Canada.

Zohrabyan, V., Braml, T., Keuser, M., Zircher, T. (2020). *The residual load bearing capacity of reinforced concrete as well as steel fiber reinforced concrete components after contact detonation.* 18th ISIEMS, Panama City Beach, Florida USA, October 21-25 2020.

Zukas, J. A. (Ed.) (1990). *High velocity impact dynamics*. New York: John Wiley & Sons.